Nano Energy 28 (2016) 29–43

Contents lists available at ScienceDirect

Nano Energy

journal homepage: www.elsevier.com/locate/nanoen

Recent developments of carbon-based electrocatalysts for hydrogen evolution reaction

Weijia Zhou [a,c,*], Jin Jia [a], Jia Lu [a], Linjing Yang [a], Dongman Hou [b], Guoqiang Li [b,**], Shaowei Chen [a,d]

[a] New Energy Research Institute, School of Environment and Energy, South China University of Technology, Guangzhou Higher Education Mega Center, Guangzhou, Guangdong 510006, China
[b] State Key Laboratory of Luminescent Materials and Devices, Engineering Research Center on Solid-State Lighting and its informationisation of Guangdong Province, South China University of Technology, 381 Wushan Road, Guangzhou 510641, China
[c] Guangdong Provincial Key Laboratory of Atmospheric Environment and Pollution Control, South China University of Technology, Guangzhou Higher Education Mega Centre, Guangzhou 510006, China
[d] Department of Chemistry and Biochemistry, University of California, 1156 High Street, Santa Cruz, CA 95064, United States

ARTICLE INFO

Article history:
Received 18 April 2016
Received in revised form
14 July 2016
Accepted 9 August 2016
Available online 10 August 2016

Keywords:
Carbon-based electrocatalysts
Nonmetal doping
Core-shell structure
Electronic state density
Hydrogen evolution reaction

ABSTRACT

Development of effective technologies for clean and sustainable hydrogen energy has been attracting great attention. Toward this end, an effective and promising approach is based on the electrolysis of water for hydrogen production. To date, the most effective hydrogen evolution reaction (HER) electrocatalysts are Pt-group metals with a low overpotential to generate large cathodic current densities. However, the high cost and scarcity severely limit their broad utilization. As alternatives to Pt electrocatalysts, transition metal compounds as effective HER catalysts have been prepared in a series of recent studies. However, thus far, it remained a great challenge to develop highly active HER catalysts with a low overpotential based on earth-abundant and cost-effective materials. Recently, the new significant developments about carbon-based electrocatalysts with a low overpotential toward HER have stimulated a great deal of the researchers' interest. In particular, the catalytic activity of carbon based-catalysts can be enhanced by transition metal nanoparticles as core and nonmetal doping into carbon skeleton, which can modulate the electronic state density of carbon to produce new active sites for HER. In this feature article, we review the research progress in the development of carbon-based electrocatalysts toward HER in acid electrolytes throughout the past few years. In addition, some notable matters and challenge in the research of HER are discussed in this review.

Contents

* Corresponding author at: New Energy Research Institute, School of Environment and Energy, South China University of Technology, Guangzhou Higher Education Mega Center, Guangzhou, Guangdong 510006, China.
** Corresponding author.
E-mail addresses: eszhouwj@scut.edu.cn (W. Zhou), msgli@scut.edu.cn (G. Li).

http://dx.doi.org/10.1016/j.nanoen.2016.08.027
2211-2855/

1. Introduction

Development of effective technologies for clean and sustainable hydrogen energy has been drawn increasing attention in the past few years, as hydrogen is hailed as a promising energy source to reduce our dependence on fossil fuels and benefit the environment by reducing the emissions of greenhouse and other toxic gases. Toward this end, an effective and promising approach is based on the electrolysis of water for hydrogen production. Electrocatalytic hydrogen evolution reaction (HER) preferably driven by solar energy is a highly attractive methodology for meeting these requirements [1–3]. Yet such a promise will be realized only when the production can be carried out in an efficient, low-cost, and environmentally friendly fashion. As shown in the equation: $H^+ + \text{catalyst} + e^- = \text{catalyst-H}$ (acid solution), the catalyst need only adsorb free H^+ ion in acidic electrolytes. But, as shown in the equation: $H_2O + \text{catalyst} + e^- = \text{catalyst-H} + OH^-$ (alkaline solution), the catalyst need break the H–O–H bonding in alkaline electrolytes before adsorbing H^+ ion. So, the acidic electrolytes (e.g. 0.5 M H_2SO_4) are preferred for water electrolysis to produce hydrogen as there are enough H^+ ions in the electrolyte to react on the electrode surface. In addition, hydroxide-conducting polymeric electrolytes are still in their technological infancy: they are unstable and less conductive than their proton-conducting counterparts and impose greater overpotentials for HER [4]. Therefore significant research efforts have been devoted to the design and engineering of acid-stable HER catalysts.

To date, Pt-based electrocatalysts are known to efficiently catalyze HER, while their widespread use has been limited by their low earth-abundance and high-cost; hence, the development of HER catalysts that are composed of inexpensive and earth-abundant elements has been one of the main targets in renewable energy research in recent years [5–9]. Molybdenum- and transition-metal-based compounds are an exciting family of HER catalysts, including MoS_2 [10–12], $MoSe_2$ [13], Mo_2C [14], MoP [15], WS_2 [16], $CoSe_2$ [17], CoS_2 [18], CoP [19,20], NiP [2], M_3C (M: Fe, Co, Ni) [21], which exhibit excellent activity and robust stability in acidic electrolytes. Recently, the studies about carbon-based catalysts with low overpotentials for HER have stimulated a great deal of interest. The pristine carbon materials are electrochemically inert or possess the poor catalytic activity [22–25]. This is the basis that we can use various carbon-based current collectors such as glassy carbon, carbon paper and carbon cloth in electrochemical experiments. Chemical modification of the carbon surface is usually necessary in order to enhance its electrocatalytic activity [26]. Actually, the electronic state density of carbon may be modulated by transition metal nanoparticles [22,27,28] and nonmetal doping [28–30], such that carbon may serve as active sites for HER. As a rising category of potential candidates for the replacement of Pt-based catalysts, carbon-based materials are considered to have great potential to solve some vital issues for HER. Up to now, there are two main kinds of carbon-based electrocatalysts: (1) nonmetallic elements doped carbon and (2) the metal@carbon core-shell structures. Recent rapid increases of carbon based electrocatalysts for HER have motivated demand for reviewing of this research field. To the best of our knowledge, although some investigations or reviews involving transition metal based, especially molybdenum-based compounds as HER catalysts have been reported [31–38], comprehensive reviews about carbon-based electrocatalysts for HER are still rare [39]. This review summarizes recent achievements in carbon based electrocatalysts for HER, and beneficial to future development of other novel low-cost catalysts with high activities and long lifetimes for practical applications. Additionally, some notable matters and challenge in the electrochemical measurement of HER are discussed in this review.

2. Nonmetal doped carbon for HER

Hetero-atoms (e.g. N, S, P, B or others) as dopant into carbon can modulate carbon's physical and chemical properties to obtain more reactive sites. More importantly, this process can produce carbon-based materials with improved ability to adsorb the atomic/molecular species undergoing catalytic reactions and without substantially compromised conductive properties [40]. These types of heteroatoms doped structures may provide opportunities for further developing low-cost metal-free catalysts with high activities and long lifetimes. It has been known that the difference in electronegativity and size between the hetero-atoms (N, P, B, and S) and carbon can polarize adjacent carbon atoms to facilitate oxygen reduction reaction (ORR) [41–43], which may be applicable to the hydrogen evolution process [24,28,44]. The HER performances of heteroatom-doped carbon metal-free catalysts are summarized in Table 1.

2.1. Nitrogen-doped carbon for HER

Nitrogen containing carbons have received increasing interest as they can improve the properties of carbon for various applications, including ORR [51] and photocatalysis [52]. When nitrogen atoms are introduced into the carbon structure, the electrical conductivity, basicity, oxidation stability, and catalytic activity of carbon can be altered. The performance of these materials crucially depends on the amount of nitrogen in the carbon host as well as its local structure. However, the N doped carbons as efficient catalysts for HER have rarely been reported [48,53,54]. Antonietti et al. [53] reported that the carbon nitride (C_3N_4) electrodes show high HER activity with low overpotential and acceptable current densities due to an enhanced H adsorption (Volmer step). Qu et al. reported that hierarchical architecture of graphitic carbon nitride (g-C_3N_4) nanoribbon-graphene provides a large accessible surface area, multi-electron transport channel and short diffusion distance for an excellent charge separation and transfer, that effectively accelerates the electrochemical process for HER [47]. As shown in Fig. 1, Qiao et al. synthesized a flexible three-dimensional (3D) film by integrating porous C_3N_4 nanolayers with nitrogen-doped graphene sheets, which can be directly utilized as

Table 1
Summary of heteroatom-doped metal-free catalysts for HER.

Heteroatom-doped carbon	Methods	Doping elements	Onset potential (mV vs. RHE)	Tafel slope (mV dec^{-1})	η (V vs. RHE) for $J=-10$ mA cm^{-2}	Refs.
g-C_3N_4 nanoribbon-graphene	a one-step hydrothermal melamine	N	80	54	0.207	[45]
Porous C_3N_4@N-graphene-750 film	a simple vacuum filtration ammonia	N	8	49.1	0.08	[29]
B-substituted graphene	a facile wet chemical synthetic BH_3-THF	B	200	99	–	[40]
N, S doped carbon-500	chemical vapor deposition pyridine thiophene	N, S	130	80.5	0.28	[30]
N, S doped carbon	thermal decomposition peanut root nodules	N, S	27	67.8	–	[28]
N, P doped graphene	chemical -doping melamine triphenylphosphine	N, P	289	91	0.422	[24]
g-C_3N_4@S–Se-pGr	in situ process sulfur and selenium powder	S, Se	92	86	–	[46]
N doped hexagonal carbon	chemical vapor deposition N_2	N	65	56.7	0.18	[47]
N doped carbon	a micelle-template cyanamide	N	–	109	0.239	[48]
C_3N_4@N doped graphene	anneal dicyandiamide	N	–	51.1	0.24	[49]
N, S doped carbon-800	simple pyrolysis human hair	N, S	12	57.4	0.097	[28]
N, P doped carbon	carbonizing Staphylococcus aureus	N, P	76	58.4	0.204	[50]

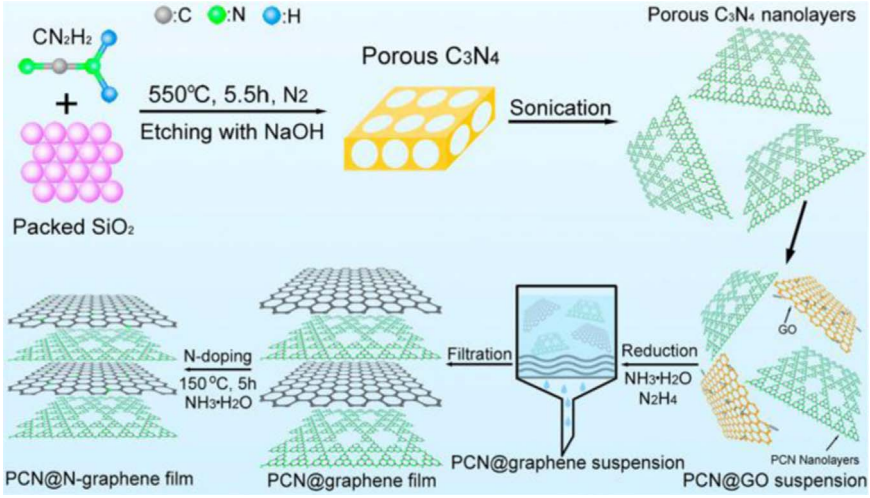

Fig. 1. Schematic illustration of the preparation process of PCN@N-graphene film. (Reprinted with permission from Ref. [29] ©2015 American Chemical Society.)

HER catalyst electrodes without substrates, which possessed highly exposed catalytic centers, hierarchical pores and strong mechanical flexibility [29]. The electrochemical measurement showed that 3D heterostructured electrodes possess the efficient catalytic activity for HER, onset potential (−8 mV vs. RHE) close to that of commercial Pt (0 mV vs. RHE @ 0.5 mA cm^{-2}), high exchange current density of 0.43 mA cm^{-2}, and remarkable durability (seldom activity loss >5000 cycles).

2.2. Other heteroatom (B, S) doped carbon for HER

Researches involving the electrocatalytic activities of carbon materials doped with other low (e.g. B) [55] or similarly (e.g. S) [40] electronegative atoms have attracted increasing attention. Asefa et al. reported a facile wet chemical synthetic method to electrocatalytically active, B-substituted graphene, which as an efficient metal-free electrocatalyst for HER showed onset potential of −200 mV vs. RHE with Tafel slopes of ~99 mV dec^{-1}. In addition, Amini et al. [56] succeeded in synthesizing the sulfur doped graphene nanosheets, which showed enhanced activity for HER. The S dopants introduced the structure defects into the graphene lattice to form the S–C bonding, which appeared to be related to the active sites for HER. Lees's group reported the molecularly designed and metal-free catalysts synthesized by coupling a g-C_3N_4 with graphene doped by S, Se, or S-Se (Fig. 2) [46]. In our group, sulfur and nitrogen self-doped carbon nanosheets were prepared as efficient non-metal catalysts for HER by thermal decomposition of peanut root nodules (an abundant biowaste). Electrochemical measurements showed apparent electrocatalytic activity for HER in 0.5 M H_2SO_4, with a small overpotential of only 27 mV, a Tafel slope of 67.8 mV dec^{-1} and good catalytic stability [28].

2.3. Dual or treble doped carbons in metal-free catalysts

After single heteroatom doping had been confirmed to improve the electrocatalytic performance of carbon materials, development of carbon materials doped with dual heteroatoms motivated the curiosity. For example, B/N, S/N and P/N couples could lead to the unique electron-donor property by the synergistic coupling effect

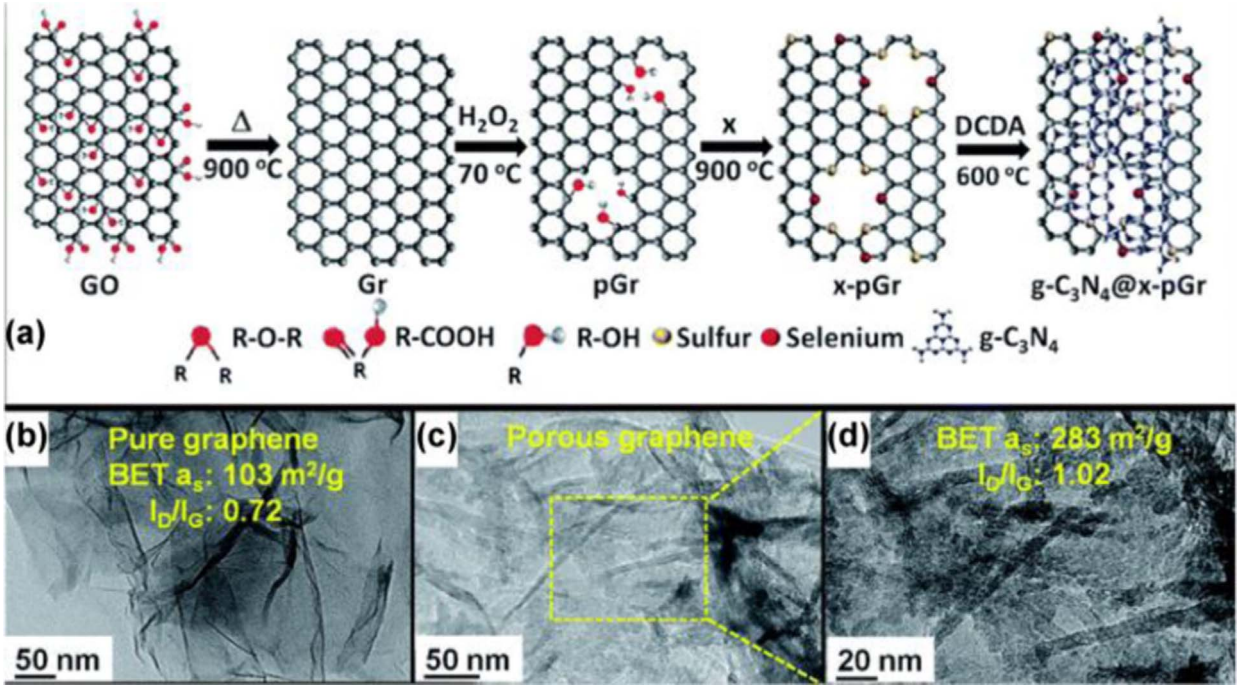

Fig. 2. (a) Schematic representation of the growth of g-C_3N_4@*x*-graphene (*x*=S, Se, S-Se). TEM images of (b) pure graphene and (c and d) nanoporous graphene. (Reprinted with permission from Ref. [46] ©2015 The Royal Society of Chemistry.)

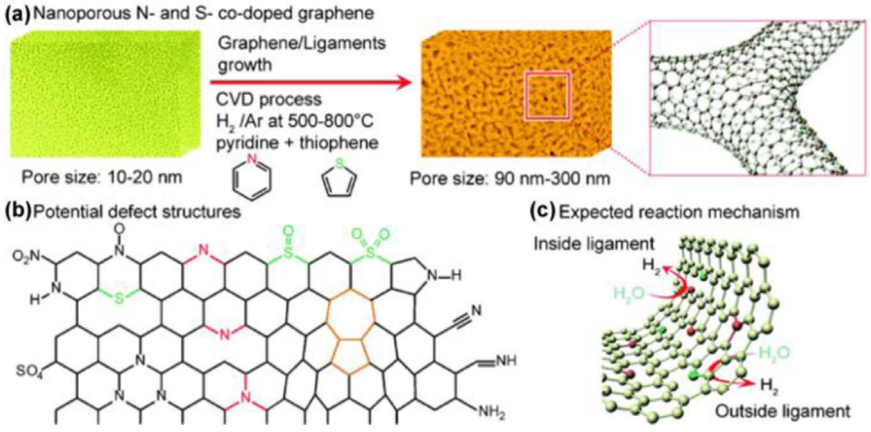

Fig. 3. Illustration of the preparation process of N and S co-doped nanoporous graphene. (a) Preparation of nanoporous N,S-doped graphene by CVD. (b) Potential defect structures in NS-doped nanoporous graphene. (c) Expected reaction mechanism on nanoporous graphene. (Reprinted with permission from Ref. [30] ©2014 Wiley-VCH.)

between two heteroatoms. Chen et al. prepared nitrogen and sulfur co-doped nanoporous graphene by nanoporous Ni-based chemical vapor deposition (Fig. 3) [30]. The obtained nitrogen and sulfur co-doped nanoporous graphene leaded to high catalytic activity for HER with an onset potential of −130 mV vs. RHE, Tafel slope of 80.5 mV dec^{-1} and operating potential of −280 mV@ 10 mA cm^{-2}. Qiao et al. designed and synthesized N and P dual-doped graphene by annealing graphene oxide with a melamine and triphenylphosphine mixture in an Ar atmosphere [24]. The N and P heteroatoms could co-activate the adjacent C atom in the graphene matrix by affecting its valence orbital energy levels to induce a synergistically enhanced reactivity toward HER. Electrochemical measurements (Fig. 4) showed that N and P dual-doped graphene (420 mV @10 mA cm^{-2}, 91 mV dec^{-1}) was more active than those of the single N doped graphene (490 mV, 116 mV dec^{-1}) and P doped graphene (553 mV, 133 mV dec^{-1}).

2.4. Catalytic mechanism for nonmetal-doped carbon for HER

Heteroatom doped graphene nanosheets have been explored as metal-free HER electrocatalysts, recently. To understand the underlying mechanisms of the doping enhanced HER catalysis, the density functional theory (DFT) calculations were performed to investigate the electronic structure and H* absorption free energy of electrocatalysts for HER. Using DFT calculations, Qiao et al. [24] explored several heteroatom (N, B, O, S, P and F) doped or co-doped graphene models and predicted that N and P co-doping afforded the optimal HER activity with Gibbs free-energy of the hydrogen adsorption (ΔG_H^*) of −0.08 eV. In a parallel study, Chen et al. [30] synthesized N and S co-doped nanoporous graphene by chemical vapor deposition on a Ni substrate using pyridine and thiophene as the N and S precursors. The N,S-doped graphene exhibited an onset overpotential of −130 mV and Tafel slope of 80.5 mV dec^{-1} in acid electrolytes, which was better than those of N-doped graphene and S-doped graphene (Fig. 5). Based on DFT calculations, the authors proposed that the synergistic coupling of

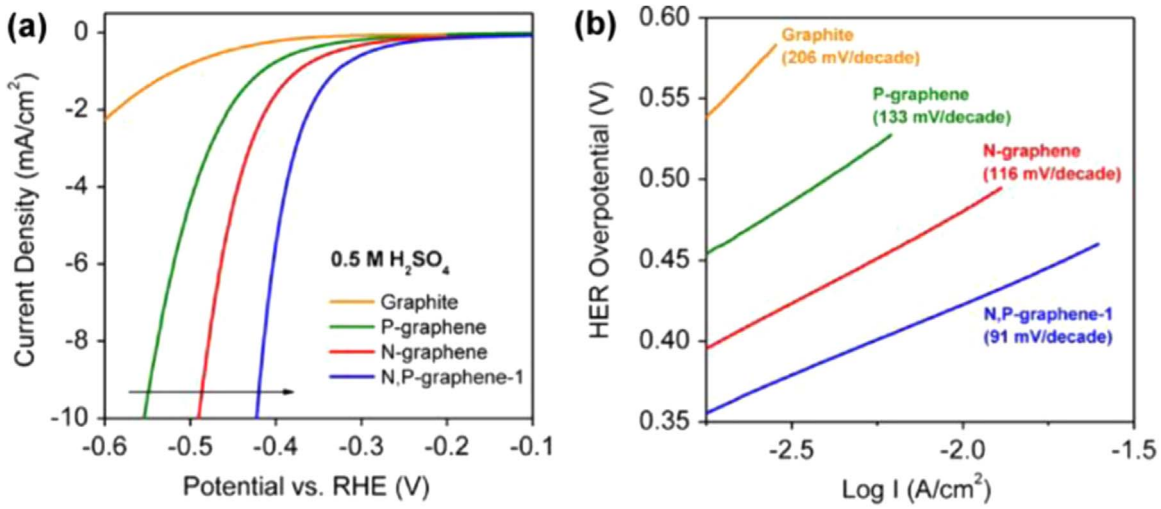

Fig. 4. (a) HER polarization curves, (b) the corresponding Tafel plots of N- and/or P-doped graphene electrocatalysts in 0.5 M H_2SO_4. (Reprinted with permission from Ref. [24] ©2014 American Chemical Society.)

S and N dopants with geometric defects in the graphene lattice reduced $|\Delta G_H^*|$ on graphene, and hence was responsible for the improved HER activity [30]. However, it's worth noting that there are some possible metal impurities (e.g. Fe, Co, Ni and Mo) in nonmetal doped carbon (such as carbon nanotubes with the metal catalyst seeds, activating agent of $MgCl_2$ and template of Ni foam), which can affect the HER activity. So, the nonmetal doped carbon electrocatalysts need more accurate evaluation.

2.5. Metal doped carbon for HER

Recently, metal atoms doped carbon with efficient HER activity has been developed, such as nanoporous graphene with single-atom nickel dopants [23] and atomic cobalt doped in N-doped graphene (Fig. 6) [57]. Chen and Tour [57] reported that very small amounts of cobalt dispersed as individual atoms on nitrogen-doped graphene possess low overpotentials (30 mV). The

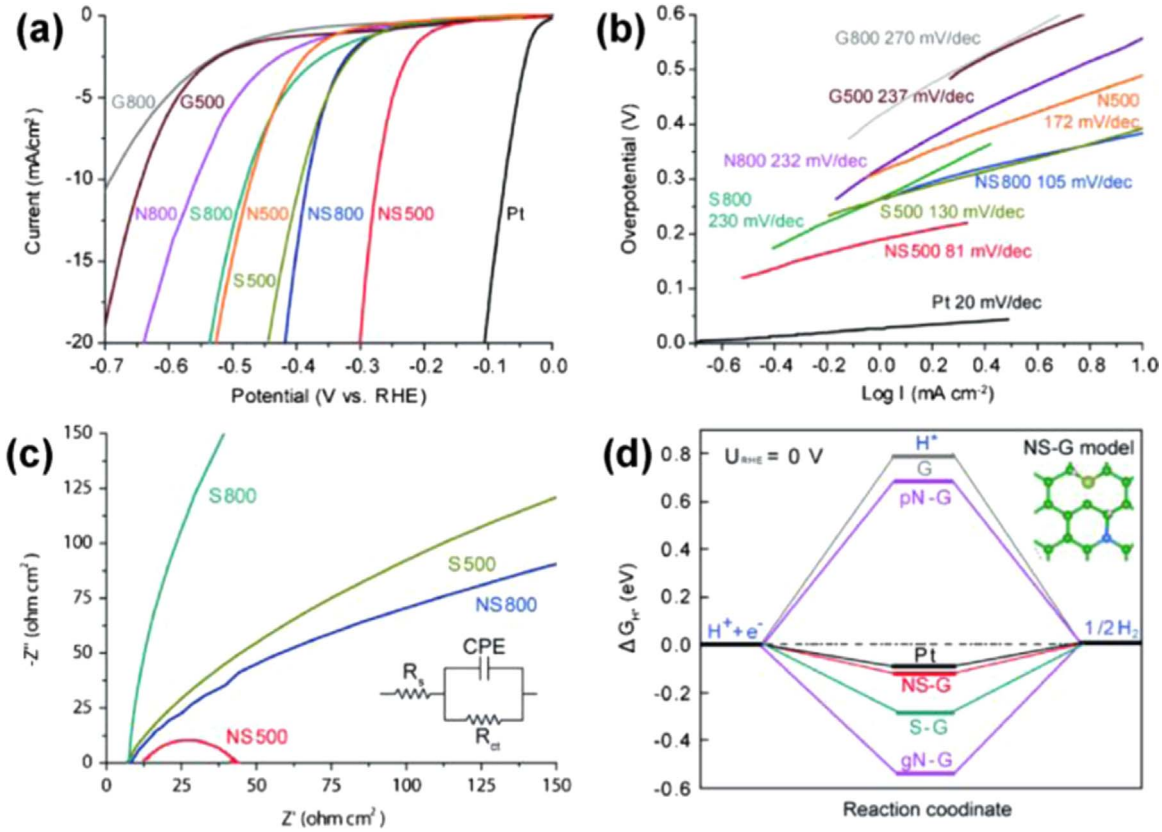

Fig. 5. HER activity of chemically doped nanoporous graphene nanosheets. (a) CV curves of the samples produced at different CVD temperatures and with different dopants in comparison to undoped nanoporous graphene. (b) Tafel plots for the different graphene samples. (c) Electrochemical impedance spectroscopy of the graphene samples at HER overpotential of 200 mV. (d) DFT-calculated HER activities of chemically doped nanoporous graphene nanosheets with a geometric lattice defect. Shown is the calculated HER free energy diagram at equilibrium potential for a Pt catalyst and for pyridinic (pN-G), graphitic (gN-G), sulfur doped (S-G), and nitrogen/sulfur co-doped (NS-G) graphene samples. The inset shows a NS-doped graphene model with a nitrogen (blue), sulfur (yellow), and hydrogen atom (white). (Reprinted with permission from Ref. [30] ©2014 Wiley-VCH.)

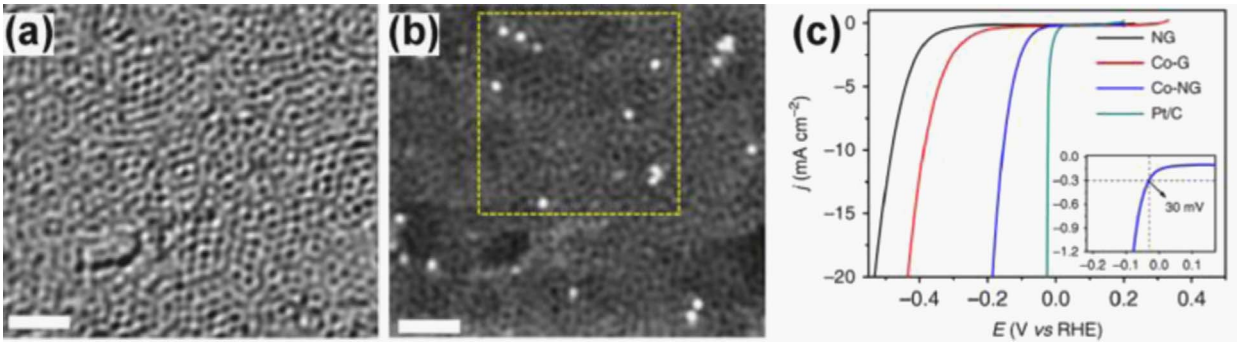

Fig. 6. (a) Bright-field aberration-corrected STEM image of the Co-NG showing the defective and disordered graphitic carbon structures. Scale bar, 1 nm. (b) HAADF-STEM image of the Co-NG, showing many Co atoms well-dispersed in the carbon matrix. Scale bar, 1 nm. (c) Polarization curves of NG, Co-G, Co-NG and Pt/C in 0.5 M H_2SO_4 at scan rate of 2 mV s^{-1}. The inset shows the enlarged view of the polarization curves for the Co-NG near the onset region. (Reprinted with permission from Ref. [57] @ 2015 Nature publishing group.)

catalytically active sites are associated with the metal centers coordinated with nitrogen. In addition, single-atom nickel dopants anchored to three dimensional nanoporous graphene shows superior HER performance with a low overpotential of approximately 50 mV and a Tafel slope of 45 mV dec^{-1} in 0.5 M H_2SO_4 solution, together with excellent cycling stability. Experimental and theoretical investigations suggest that the unusual catalytic performance of this catalyst is due to sp-d orbital charge transfer between the Ni dopants and the surrounding carbon atoms [23]. Up to now, there are many reports about nonmetal and metal doped carbons used as highly active HER catalysts. However, the accurate assessment of the catalytic sites resulting from nonmetal atoms or metal atoms in doped carbon electrocatalysts needs more an in-depth study.

3. Metals embedded in carbon for HER

The metal@carbon materials are growing attractive candidates for HER catalysts. Reports about pure metals of Co, Fe and Ni used as HER catalysts have been relatively scarce because of their chemical instability in acidic environments [58]. One approach is that building a thin carbon layer on the surface of metals, which hindered the transition metals from dissolution in acid electrolyte as well as to obtain the prominent catalytic contributions from the entrapped metal nanoparticles due to interfacial charge transfer [6,22,27,28]. Some of these efforts have already led to some efficient metal@carbon HER catalysts (e.g. Fe@carbon, Co@carbon), which possess unique stability in a wide pH range owing to the protection of carbon shell. The HER performances of metal@carbon catalysts are summarized in Table 2.

3.1. Core-shell structure for carbon nanotubes (CNTs) and nanoparticles

Cobalt-embedded nitrogen-rich carbon nanotubes (Co-NRCNTs) were synthesized by Zou et al. (Fig. 7) [22], which served as highly active electrocatalyst for HER with a small onset potential of −50 mV vs. RHE and a smaller Tafel slope (69 mV dec^{-1}) at pH 0. The results have guided to synthesize all kinds of metal@carbon electrocatalysts for HER [6,20–22,27,28,59,61,63–67]. The core metals (Fe, Co, Ni and alloy) [59,64,66,67], carbon shell (dicyandiamide [61], urea [66], EDTA [59], and cellulose filter [67]) and nanostructures (nanotubes [6,61], and nanoparticles [27]) have been considered to affect the HER activity of metal@carbon catalysts. Research progress was summarized below: (1) Up to now, the core metals have been restricted to only a small number of transition metals, such as Fe, Co and Ni. Extending the core metal to other metals is the important research content in the future [25,68,69]. (2) The nonmetal doping into carbon shells synergistically increases the electron density on the graphene surface, which resulted in superior HER activity. Up to now, only N doping into metal@carbon with enhanced HER activity have been reported [22]. The other elements, such as S and P, doped into

Table 2
Summary of metal@carbon catalysts for HER in acid electrolyte.

metal@carbon catalysts	Morphologies	Metal core	Onset potential (mV vs. RHE)	Tafel slope (mV dec^{-1})	η (mV vs. RHE) for $J=-10$ mA cm^{-2}	Refs.
FeCo@N-doped Carbon nanotubes-NH_3	Tubular	FeCo	~−70	63	~270	[6]
Cobalt-embedded nitrogen-rich CNTs	Multi-wall carbon Nanotubes	Co	−50	69	260	[22]
CoNi@N-doped Carbon	Nanospheres	CoNi	~0	105	142	[59]
Co-embedded Nitrogen-doped CNT/Carbon Cloth	Nanowire array	Co	–	74	78	[60]
Co_3O_4@ Graphitic Carbon Nitride-5%$CoCl_2 \cdot 6H_2O$-450 °C	Tubular	Co_3O_4	−30	–	90	[61]
CoP-Ordered Mesoporous Carbon	Nanorods	CoP	−77.74	56.7	112	[20]
Co@N-Doped Carbon/ N-Doped Graphene	Wrinkled surface	Co	−49	79.3	200, J=−13.6	[62]
Co@Nitrogen-doped Graphene Films	Layer alternate	Co	−14	93.9	~125	[63]
Co@N-doped carbon/Ti mesh	Nanorod arrays	Co	−56	78.2	106	[28]
Fe_3C-Graphene Nanoribbons Co_3C-Graphene Nanoribbons	Vertically aligned Graphene nanoribbons	Fe_3C	−32	46	200, $J=166.6$	[21]
		Co_3C	−41	57	200, $J=79.6$	
Ni_3C-Graphene Nanoribbons		Ni_3C	−35	54	200, $J=116.4$	
Single-shell Carbon-Encapsulated Iron Nanoparticle/Single-walled Carbon Nanotube	Single-shell carbon-encapsulated iron nanoparticles	Fe	~0	40	77	[64]

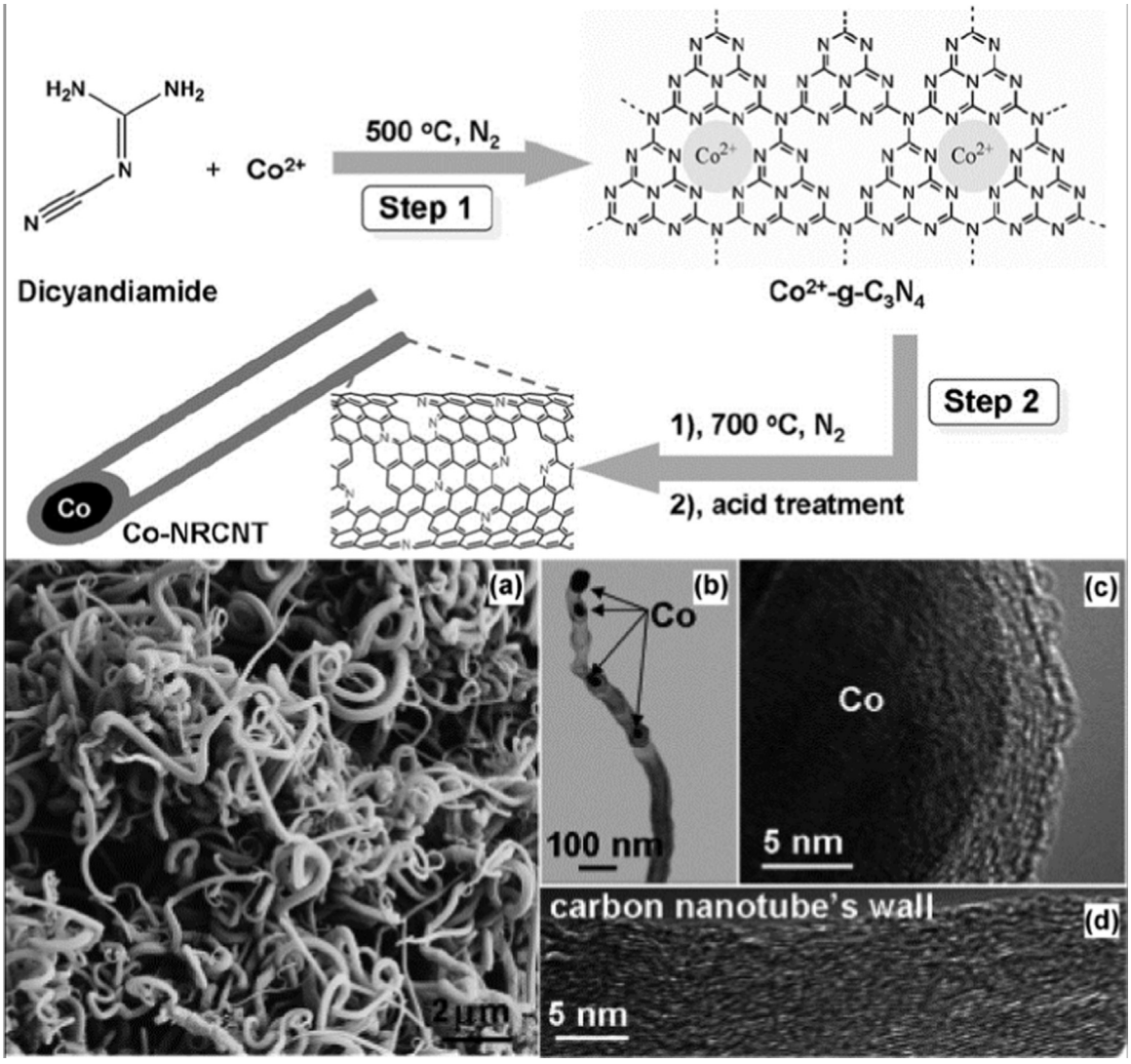

Fig. 7. Synthesis of Co-NRCNTs: Step 1: thermal treatment at 500 °C in N_2 atmosphere of a mixture of dicyandiamide and $CoCl_2 \cdot 6H_2O$ to form Co^{2+}-g-C_3N_4. Step 2: additional thermal treatment at 700 °C in N_2 atmosphere of the Co^{2+}-g-C_3N_4, followed by acid treatment of the resulting material to etch away any accessible cobalt species on it. (a) SEM image, (b–d) STEM images of Co-NRCNTs. (Reprinted with permission from Ref. [22] ©2014 Wiley-VCH.)

carbon shell with high HER activity have been not reported. (3) DFT calculations indicate that the ultrathin graphene shells (less than 2 nm) promote electron penetration from the metal core to the graphene surface to enhance the HER activity. Deng et al. [59] designed a hierarchical architecture consisted of CoNi nanoalloy encapsulated by 1–3 layers of ultrathin graphene shells (CoNi@NC), which prepared by a bottom-up method of using Co^{2+}, Ni^{2+}, and $EDTA^{4-}$ as precursors. The optimized catalyst exhibited high stability and activity with an onset overpotential of almost zero vs. RHE and an overpotential of only 142 mV at 10 mA cm^{-2}, which was quite close to that of commercial 40% Pt/C catalysts in 0.1 M H_2SO_4 electrolyte (Fig. 8). Up to now, it is supposed that the catalytic sites of metal@carbon locate on carbon shell, resulting from the electron injection by core metals. In fact, experiments confirmed that the nonmetal-doping in carbon shell is vital to enhance the HER activity of metal@carbon and the metal cores encapsulated by pure carbon possessed the poor HER performance [62]. This is because that the hetero-atoms doping into carbon shell will introduce the structure defects into the graphene lattice, which weaken the limit of carbon shell thickness. However, the catalytic mechanisms of metal@carbon require in-depth research.

According to the above mechanism, the HER catalytic sites of metal@carbon were located on the surface of carbon shell, which increased with the interface between metal core and carbon shell. So, the various metal@carbon structures loaded onto grapheme [65], carbon nanotubes [22], cellulose filter paper [67] and Ti mesh [28] have been reported. For examples, Mohammad Tavakkoli et al. [64] prepared single shell carbon-encapsulated iron nanoparticles (SCEINs) decorated on single-walled carbon nanotubes (SWNTs) as a novel highly active and durable non-noble-metal catalyst for the HER (Fig. 9), which possessed a low overpotential of 77 mV to achieve current densities of 10 mA cm^{-2} with a Tafel slope of 40 mV dec^{-1}. Zhou et al. [62] reported that N-doped carbon-wrapped cobalt nanoparticles supported on N-doped graphene nanosheets (Co/NC/NG) were prepared by a facile solvothermal procedure and subsequent calcination at controlled temperatures, which possessed a small overpotential of 49 mV with a Tafel slope of 79.3 mV dec^{-1} and prominent electrochemical durability in 0.5 M H_2SO_4. The electrochemical results confirmed that the synergetic effect among N-doped graphene, metal Co, and core-shell structure played an important role in enhancing HER activity (Fig. 10).

Notably, to develop high efficiency and binder-free HER electrodes, active components are directly grown on current-collecting substrates instead of using Nafion as binder. The 3D electrode

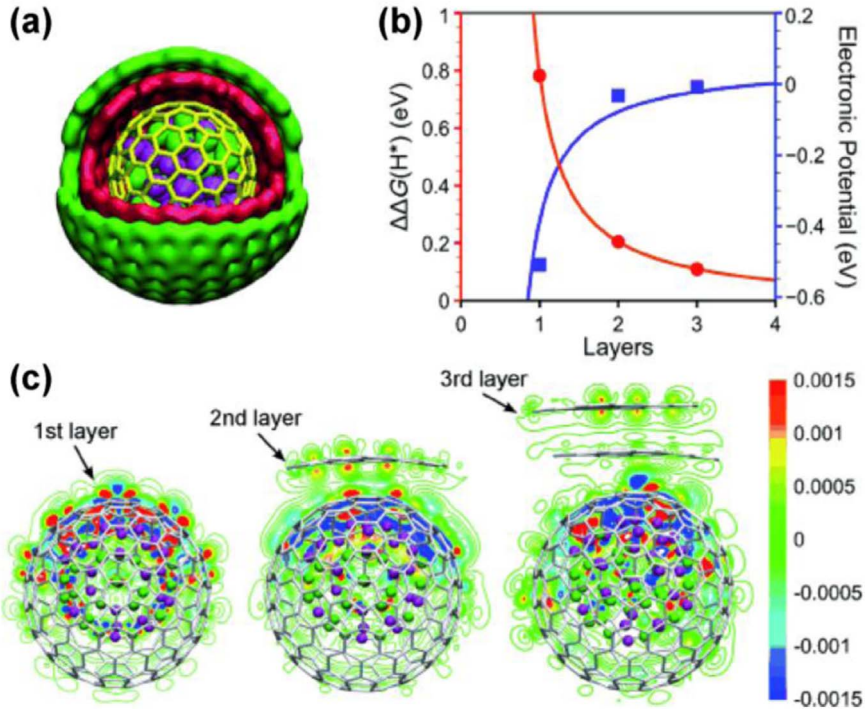

Fig. 8. (a) Schematic illustration of a CoNi alloy encapsulated in three-layer graphene. (b) ΔΔG(H^*) (red line) and electronic potential (blue line) as a function of the number of graphene layers, where ΔΔG = ΔG (without metal)-ΔG (with metal). (c) Redistribution of the electron densities after the CoNi clusters have covered by one to three layers of graphene. The differential charge density ($\Delta\rho$) is defined as the difference in the electron density with and without the CoNi cluster. The red and blue regions are regions of increased and decreased electron density, respectively. (Reprinted with permission from Ref. [59] ©2014 The Royal Society of Chemistry.)

entailed a large surface area and abundant exposed active sites. For example, Zhou et al. [28] described the preparation of self-supported N-doped carbon-coated cobalt nanorod arrays supported on a Ti mesh (Co@NC/Ti, Fig. 11), which exhibited a remarkable HER performance in acid solutions with an onset potential of −56 mV vs. RHE, a Tafel slope of 78.2 mV dec^{-1}, and robust stability for 8 h of continuous operation. In addition, Xing et al. [27] described the direct growth of a film consisting of interconnected Co-entrapped, N-doped carbon nanotubes on carbon cloth using chemical vapor deposition from dicyanodiamine using a Co_3O_4 nanowire array as a flexible 3D electrode, which delivers 10, 20, and 100 mA cm^{-2} at overpotentials of 78, 100, and 155 mV in 0.5 M H_2SO_4, respectively.

3.2. Metal organic frameworks (MOFs) for HER

Metal organic frameworks (MOFs), built from metal ions and organic ligands by coordination bonds, are a family of crystalline porous solids [70]. Thanks to their particular structure, MOFs possess diverse composition, ultra-high surface area, ordered and controllable porous structure [71]. Porous carbon and metal oxide/carbon hybrid materials with the morphology of MOFs can get easily by direct pyrolysis of MOFs under an inert atmosphere. For this reason, MOFs derived electrocatalysts have been bring in energy conversion and storage applications and exhibit excellent electrochemical activity, like supercapacitors [72,73], ORR [72,74,75] and oxygen evolution reaction (OER) [74,76]. Based on this, MOFs derived materials are also potential electrocatalysts for HER.

When MOFs were used as electrocatalysts for HER, they can be divided into two groups: (1) MOFs used as electrocatalysts directly without any other procedure. Polyoxometalates-based metal organic frameworks (POMOFs) were widely utilized as electrocatalysts for HER in recent years, for the reason that they have combined the advantages of POMs and MOFs [76–78]. Other types of MOFs, like Cu-MOF [79], Co-MOF [80] are also applied as electrocatalysts for HER without calcination, which usually possess the bad catalytic stability. (2) metal@carbon materials derived from MOFs calcined at different atmosphere as electrocatalysts for HER [69,81,82]. The high catalytic activity are mainly from following reasons: ① the porous structure of carbon inherit from the MOFs with a large surface area; ② the metal@carbon core-shell structure where electron can transfer from metal to carbon to improve the catalytic activity. For instance, Hou et al. [81] prepared a nitrogen-doped graphene/cobalt-embedded porous carbon polyhedron (N/Co-doped PCP//NRGO) through the calcination of the mixture of Co-MOFs and graphene oxide under N_2 atmosphere (Fig. 12). The hybrid offering a low onset potential of 58 mV vs. RHE and Tafel slope of 126 mV dec^{-1} at acid media. Researches about MOFs-derived HER catalysts are not only limited to a handful of elements (Zn, Cu, Co), other elements (such as Mo) are also widely employed. Wu et al. [82] synthesized porous molybdenum carbide nano-octahedrons (MoC_x) by pyrolysis of a Mo-based MOFs (Fig. 13). And MoC_x nano-octahedrons are regard as efficient electrocatalyst for HER, offering a low onset potential of −25 mV in acid electrolyte and a small Tafel slope of 53 mV dec^{-1}.

In addition to the direct carbonization of MOFs, other kinds of treatments to synthesize metal compounds as electrocatalysts for HER have also been reported. Direct phosphorization of Ni-MOFs at a mild condition can transform Ni-MOFs into nickel phosphide, which was proved to be outstanding catalyst for HER in acid electrolyte. For example, Tian et al. [83] synthesized nickel phosphides (Ni_2P) derived from Ni-MOFs by NaH_2PO_2 at 275 °C in a muffle furnace, which showed excellent HER activity in 0.5 M H_2SO_4 with a low onset potential of −75 mV and a small Tafel slope of 62 mV dec^{-1}.

4. Electrochemistry

The parameters to evaluate HER performance of

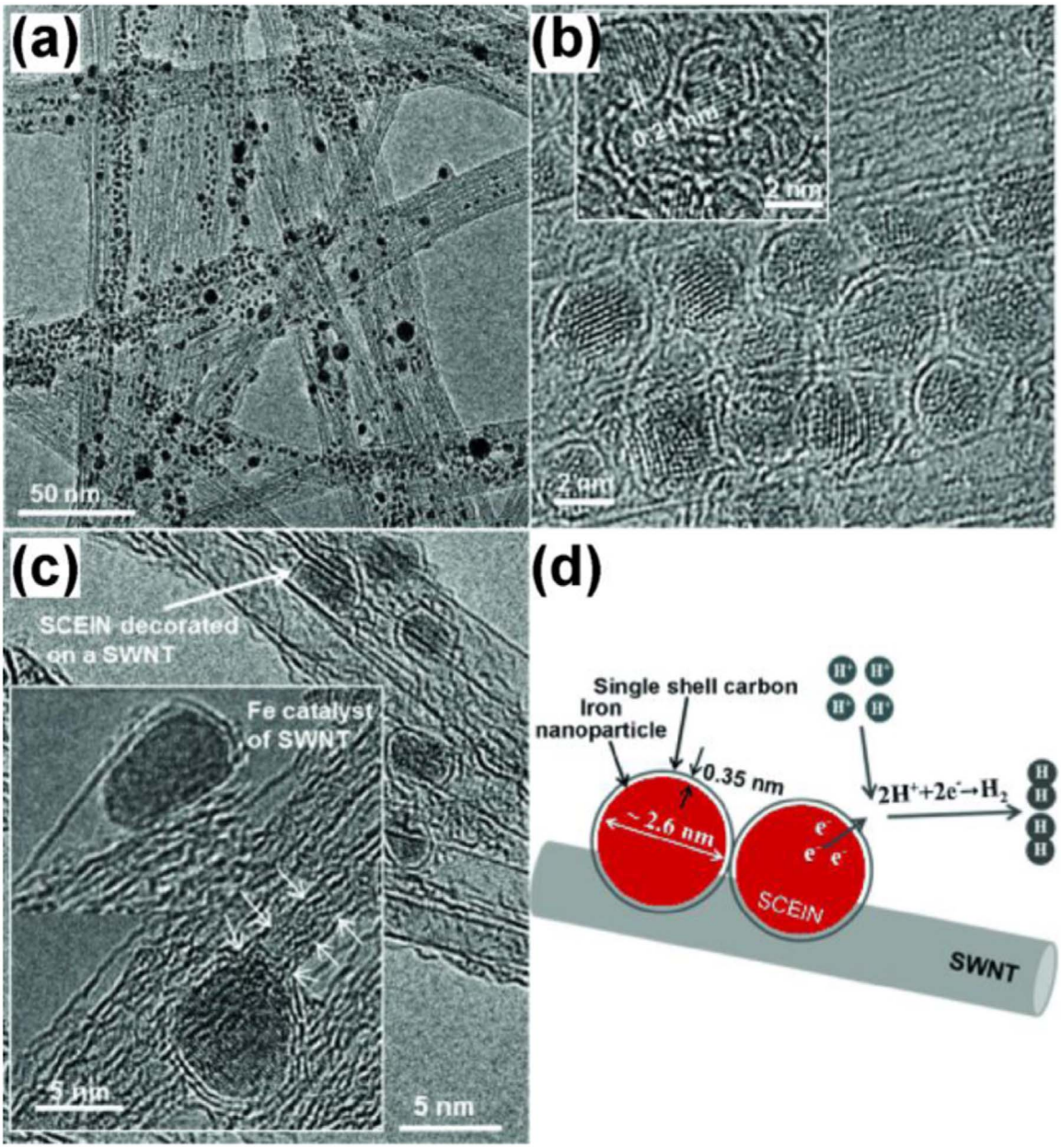

Fig. 9. (a) TEM image of single-shell carbon-encapsulated iron nanoparticles (SCEINs) supported on SWNTs showing distribution of the particles on the SWNTs. (b) HRTEM image of the SCEIN/SWNT sample, the inset indicates the (110) lattice plane of the Fe particles in SCEINs. (c) HRTEM image of SCEINs decorated on the sidewalls of the SWNTs, the inset shows Fe catalyst particles for the growth of the SWNTs (arrows demonstrate the SWNT). (d) Schematic representation of SCEIN/SWNT sample simplifying the HRTEM images and HER on SCEINs. (Reprinted with permission from Ref. [64] ©2014 Wiley-VCH.)

electrocatalysts include overpotential, current density, Tafel plot, impendence, electrochemical surface area and stability, etc. However, electrochemical measurements of carbon-based electrocatalysts for HER should be rigorously evaluated to avoid possible errors.

4.1. Overpotential/onset-potential and calibration

To conduct electrochemical water splitting, the voltages above the thermodynamic potential values corresponding to the intrinsic activation barriers present in two half reactions were known as overpotential (η) and onset potential [84,85]. The onset potential is the applied potential with apparent cathodic currents. However, it is embarrassed to determine the precise potential required to produce a current density, which usually is 0.5 or 1 mA cm^{-2}. For the further quantitative comparison of HER activity, the required overpotential to receive a current density of 10 mA cm^{-2} were widely used to evaluate the activities of the electrocatalysts in recently reports [80,81]. In fact, the measured voltage ($E_{electrolysis}$) is consisted of three parts: $E_{electrolysis} = E_{reversible} + \Delta E_{irreversible} + IR$. The $\Delta E_{irreversible}$ is the overpotential (η) for HER. Thus, in order to measure the accurate overpotential (η), the potential sweep rate of polarization curve should be measured by low sweep rate (such as 2 or 5 mV s^{-1}) to minimize the capacitive current, especially for 3D electrode with high electrochemical surface area.

In all measurements, the reference electrodes (Ag/AgCl or Hg/Hg_2Cl_2) should be calibrated with respect to a reversible hydrogen electrode (RHE). The revision process should be done at regular intervals due to the possible potential shift of reference electrodes. One method is experimental measurement. The calibration was performed in a high-purity H_2 (99.999%) saturated electrolyte with Pt wires as the working electrode and counter

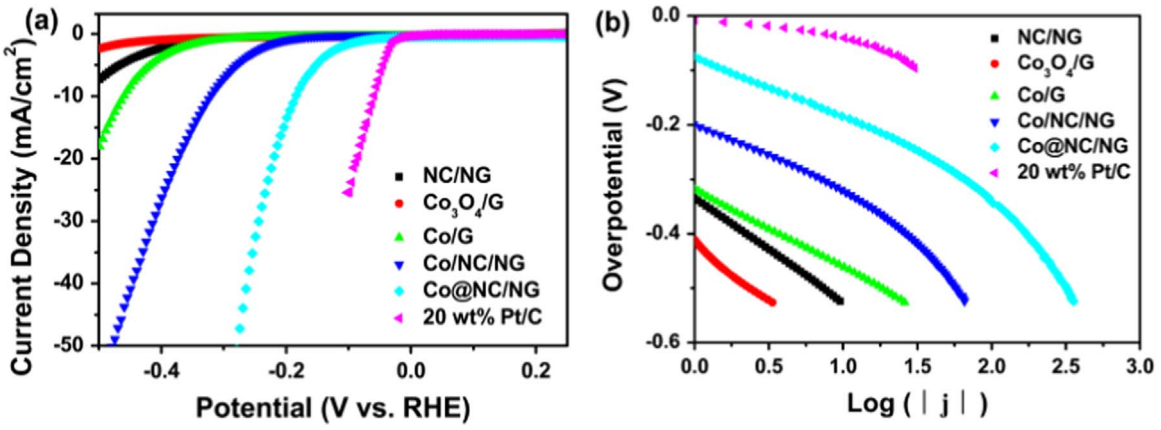

Fig. 10. (a) Polarization curves for HER in 0.5 M H_2SO_4 at a glassy carbon electrode modified with N doped carbon/N doped graphene (NC/NG), Co_3O_4 loaded on graphene (Co_3O_4/G), Co loaded on graphene (Co/G), Co loaded on N doped carbon/N doped graphene (Co/NC/NG), Co@N doped carbon/N doped graphene (Co@NC/NG) (700 °C), and 20 wt% Pt/C, respectively. Potential sweep rate 5 mV s^{-1}. (b) Corresponding Tafel plots derived from (a). (Reprinted with permission from Ref. [62] ©2015 The Royal Society of Chemistry.)

electrode. Cyclic voltammograms (CVs) were collected at a scan rate of 1 mV s^{-1}, and the average of the two potentials at which the current crossed zero was taken as the thermodynamic potential for the reversible hydrogen electrode. The other method is theoretical calculation by Nernst equation.

$$2H^+(aq) + 2e^- \rightleftharpoons H_2(g) \quad H^+|H_2(g)\,|Catalysts$$

$$E = E^\theta - \frac{RT}{nF}\ln\frac{[H^+]^2}{1} = E^\theta - 0.059pH$$

$$E^\theta(Hg/Hg_2Cl_2,\ \text{saturated KCl}) = 0.242\ V$$

$$E^\theta(Ag/AgCl,\ \text{saturated KCl}) = 0.197\ V$$

where the pH of 0.5 M H_2SO_4 is 0.3, R is the universal gas constant, $R=8.314\ \ 472\ J\,K^{-1}\,mol^{-1}$, T is the absolute temperature ($T=298.15$ K), F is the Faraday constant, the number of coulombs per mole of electrons ($F=9.648\ 533\ 99\times10^4\ C\,mol^{-1}$), n is the number of moles of electrons transferred in the cell reaction or half-reaction ($n=2$).

4.2. Current density and electrochemical surface area

It is noting that the current densities (mA cm^{-2}) of powder catalyst and block 3D electrode are achieved by two different testing methods. The former is that a certain amount of catalyst was loaded onto a glass carbon electrode (GCE), and the corresponding area is known as geometry area. The latter is, for block 3D electrode, geometric area of electrodes is also used to calculate current density. In fact, their mass loading of catalyst and actual electrochemical area are far more than those of powder catalysts loaded onto GCE. In addition, IR-compensation can exclude the influence of the resistance (Rs) from electrochemical workstation and electrode, which will increase the current density. The obtained results are useful to study the catalytic mechanism, such as the calculation of Tafel plots. However, the current density obtained without IR-compensation can give the integral and actual HER performance of electrodes.

The electrochemical surface area is employed as an approximate guide for surface roughness within an order-of-magnitude accuracy [86]. To estimate the effective surface areas, the capacitance of the double layer at the solid-liquid interface was measured. CVs were collected in a certain potential window without faradaic processes [17,85]. The current density of CV consists of two parts: capacitance current (proportional to r^1, r is the sweep speed) and faradic current (proportional to $r^{1/2}$). Therefore, the sweep speed should be high enough, such as 40, 80, 120, 160, and 200 mV s^{-1} to acquire the capacitance current.

4.3. Tafel plot and exchange current density

Tafel plot is normally used to evaluate the intrinsic property of the catalysts and the efficiency of the catalytic reaction. The polarization curves are replotted as overpotential (η) vs. log current ($\log|j|$) to get Tafel plots. By fitting the linear portion of the Tafel plots to the Tafel equation ($\eta=b\log|j|+a$, the Tafel slope (b) can be achieved. Note that for hydrogen evolution in acid electrolyte on metal electrode surfaces, the mechanism typically involves the following three major reactions [85],

First is a primary H^+ adsorption step (Volmer reaction):

$$H_3O^+ + e^- \rightarrow H_{ads} + H_2O\ b = \frac{2.3RT}{\alpha F} \approx 120\ mV\ dec^{-1} \quad (1)$$

where R is the ideal gas constant, T is the absolute temperature, $\alpha \approx 0.5$ is the symmetry coefficient, and F is the Faraday constant. This step is followed by either an electrochemical desorption step (Heyrovsky reaction),

$$H_{ads} + H_3O^+ + e^- \rightarrow H_2 + H_2O\ b = \frac{2.3RT}{(1+\alpha)F} \approx 40\ mV\ dec^{-1} \quad (2)$$

or a recombination step (Tafel reaction),

$$H_{ads} + H_{ads} \rightarrow H_2\ b = 2.3RT/2F \approx 30\ mV\ dec^{-1} \quad (3)$$

Tafel slope is an inherent property of the catalyst that is determined by the rate-limiting step of the HER. For example, HER kinetic models suggest that Tafel slope of about 120, 40 or 30 mV dec^{-1} will be obtained if the Volmer, Heyrovsky or Tafel reaction is the rate-determining step, respectively [87]. Furthermore, the logarithmic current density usually deviates from linear dependence at high overpotentials, which is strongly influenced by evolved hydrogen bubbles limiting the available surface area or mass transport [17]. Therefore, Tafel plots are recorded with the linear portions at low overpotential fitted to the Tafel equation [81]. To further estimate the intrinsic activity of the electrocatalysts, the exchange current density (j_0) is determined by extrapolation of the Tafel plots to j/log(j) axis. For $\eta=b\log j+a$, the constant terms a and b are known from the Tafel plot, the η is zero, and then the j_0 is received. The large exchange current density indicates the large surface area, fast electron transfer rate, and favorable HER kinetics.

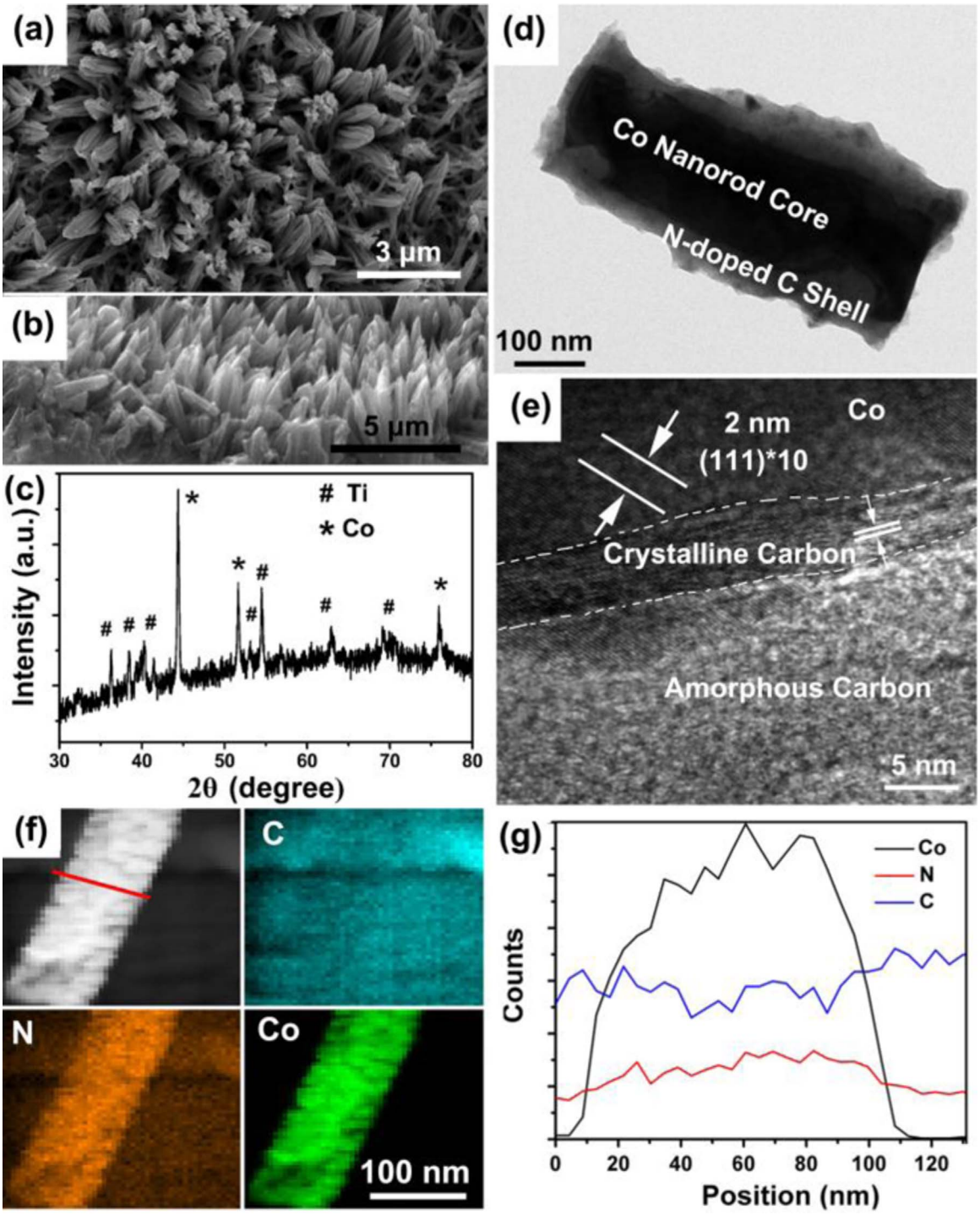

Fig. 11. (a) Top view and (b) side-view SEM images, (c) XRD patterns and (d and e) TEM images of Co@NC/Ti. (f) The corresponding EDX elemental mapping images of C, N and Co for Co@NC. (g) EDX line scan curves showing C, N, and Co element profiles across the Co@NC indicated by the red line in (f). (Reprinted with permission from Ref. [28] ©2015 The Royal Society of Chemistry.)

4.4. Electrochemical impedance

Electrochemical impedance spectroscopy (EIS) is a powerful technique to characterize interface reactions and electrode kinetics in HER. The simple equivalent circuit was usually given, where a constant phase element (CPE) was employed. The series resistance (Rs) represents a combination of ionic resistance of the electrolytes, electronic resistance of the electrode materials and internal resistance of electrochemical workstation, was obtained in the high frequency zone and then sometimes used to correct the polarization curves (IR-corrected). The charge transfer resistance (Rct) is related to the electrocatalytic kinetics and its lower value corresponds to the faster reaction rate, which can be obtained from the semicircle in the low frequency zone. From the Nyquist plots of the EIS response, we can see a depressed semicircle in the high-frequency region (Rct) and a quasi-sloping line in the low-frequency region (corresponding to mass transfer resistance). It is noting that Nyquist plots of the EIS response at various overpotentials, the diameter of the semicircles markedly diminished with increasing overpotential, suggesting decreasing

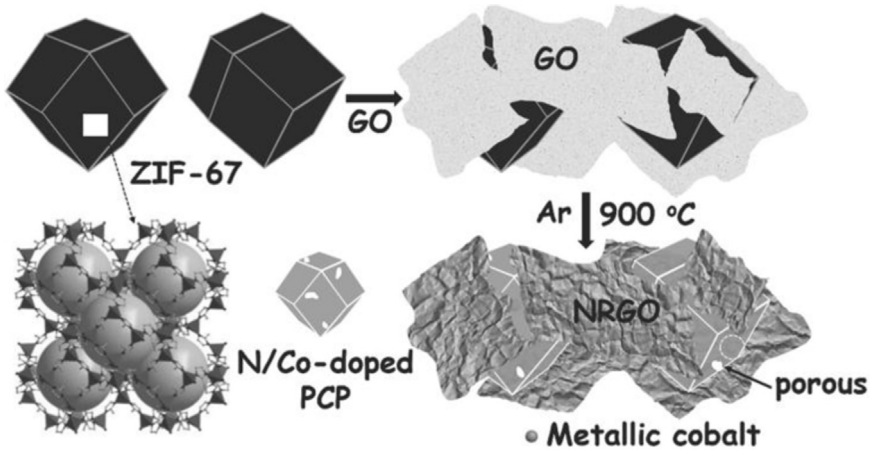

Fig. 12. Schematic illustration for the synthesis process of N/Co-doped PCP//NRGO. (Reprinted with permission from Ref. [81] ©2014 Wiley-VCH.)

Rct with increasingly negative electrode potentials.

4.5. HER durability and H_2 production

Durability is another important criterion to evaluate the HER performance of electrocatalyst. To probe the durability of the catalyst in acidic environment, long-term potential cycling and current-time responses at fixed potentials over extended periods were performed. It is noted that after continuous cyclic voltammograms at an accelerated scanning rate of 100 mV s^{-1} for 1000 cycles, the polarization curves almost exactly overlays with the initial one, with negligible loss of cathodic current [17,88]. Long-term electrochemical stability was also measured by chronopotentiometry or chronoamperometry, maintaining for a certain hours with a given current density and applied potential [89,90]. In fact, the i-t testing show the real reaction activity of hydrogen production, and the measured current densities obtained from i-t curve are usually less than or equal to that obtained from polarization curve.

The H_2 production rate was quantified by gas chromatographic measurements. Due to the increasing pressure from a large hydrogen gas production, the accurate measurement in the electrolytic cell should proceed carefully. After that, the Faradaic efficiency (FE) of the electrocatalytic hydrogen evolution process was calculated by comparing the amount of experimentally quantified hydrogen (gas chromatographic measurements) with theoretically calculated hydrogen (chronoamperometry). Faraday efficiency for HER is important information to confirm complete decomposition of water and other reductive side-reaction.

4.6. Activation

Before the testing for HER, the electrodes with cured membrane should be activated to clear the surface of electrodes and improve the hydrophilic performance. One way is the soaking the electrode in electrolyte overnight to improve the contact between catalysts and electrolyte. Another way is that given numbers of CVs were carried out, which can improve the HER activity significantly because of the improved interactions between active species and electrolyte, especially for the hydrophobic catalysts. Generally, the activation process can only increase the current density of catalysts. However, sometime, the onset potentials were significantly improved by the activation treatment. Occasionally, there are some studies claiming that “metal-free” carbon nanotubes are electrocatalytically active [91,92]. However, it should be confirmed that the high HER performance was not from the dissolution of the Pt electrode in acid electrolyte. Especially for the long time of activation process with high potentials and large current densities, the Pt electrode can be dissolved from oxidation Pt^0 to Pt^{2+}, then which is electro-reduced onto the working electrode. The other facilitating condition is the existence of chlorine ion in electrolyte from reference electrode (Ag/AgCl and Hg/Hg_2Cl_2). The results have been reported by some researchers [93,94]. When a Pt wire was used for activation process, the

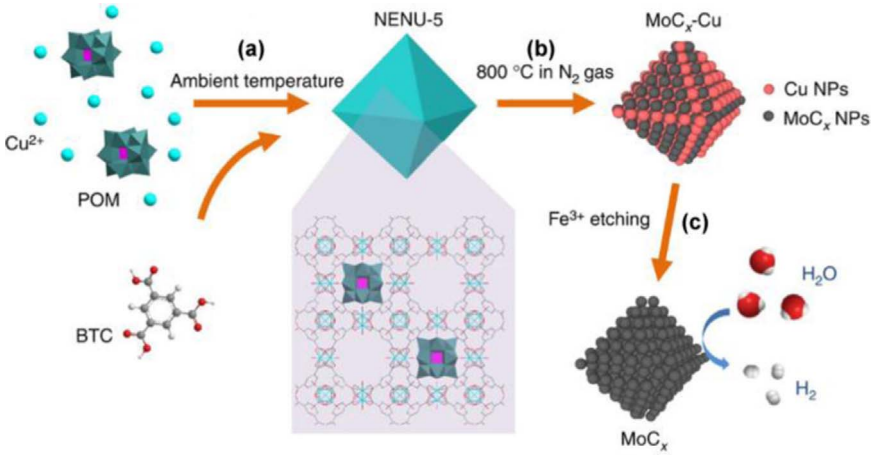

Fig. 13. Schematic illustration of the synthesis procedure for porous MoC_x nano-octahedrons. (a) Synthesis of NENU-5 nano-octahedrons with Mo based POMs residing in the pores of HKUST-1 host. (b) Formation of MoC_x-Cu nano-octahedrons after annealing at 800 °C. (c) Removal of metallic Cu nanoparticles by Fe^{3+} etching to produce porous MoC_x nano-octahedrons for electrocatalytic hydrogen production. (Reprinted with permission from Ref. [82] @2015 Nature publishing group.).

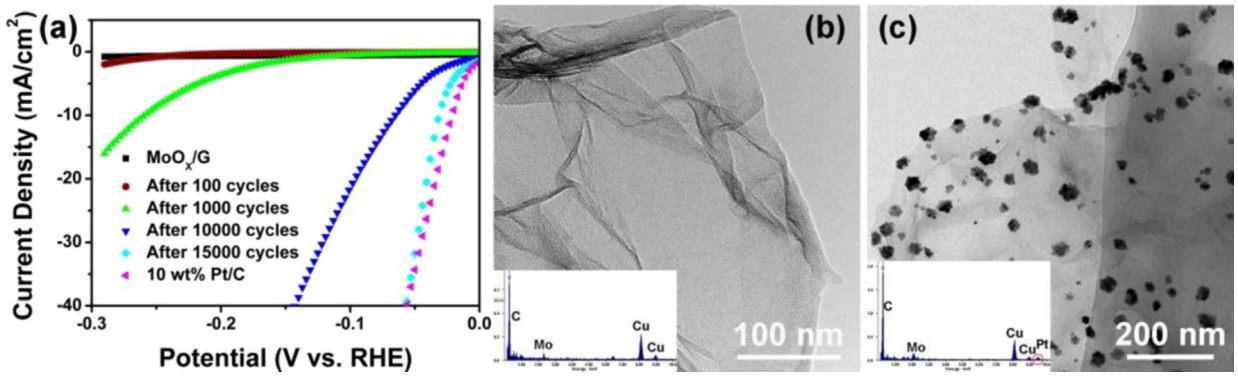

Fig. 14. (a) Polarization curves for HER in 0.5 M H_2SO_4 at a glassy carbon electrode modified with MoO_x/rGO with different activation time. Potential sweep rate of 5 mV s^{-1}. TEM images (b) and EDX (c) of MoO_x/rGO after the activation.

electrochemical catalytic activity of the graphite working electrode was greatly improved to an extent as good as that of commercial Pt/C. When a graphite rod was used, the working electrode could not be activated effectively. In our group, we also confirmed the above conclusion. The molybdenum oxide loaded on reduced graphene oxide (MoO_x/rGO) was synthesized by hydrothermal method, which was used as an electrocatalyst for HER (Fig. 14). Before activation, the MoO_x/rGO possessed the bad HER performance. After activation with different cycles, the HER performance had been improved dramatically. Fortunately, we characterized the MoO_x/rGO after activation by elemental analysis, where the apparent peaks for Pt were observed, which confirmed that the enhanced HER catalytic performance due to the dissolution of the Pt electrode in acid electrolyte.

In order to avoid the dissolution of the Pt electrode in acidic electrolyte, some measures should be employed. (1) the surface area of Pt as counter electrode should be much larger than that of working electrode; (2) the applied overpotential should not be too high; (3) avoid the presence of chloride ions in electrolyte; (4) the porous ceramic membrane between counter electrode and working electrode should be used. Actually, Pt is not indispensable as counter electrode. The counter electrode was used to balance the current and voltage from working electrode. Accordingly, as long as the materials with stability and conductive properties, can be used as counter electrode, such as Ti mesh, carbon rod and carbon cloth. (5) Pt should be not used in electrochemical measurement as an counter electrode for HER and OER in acidic electrolyte, especially under the continuous CV scan and i-t testing.

5. Outlook and future challenges

In recent years, a new family of carbon-based HER catalysts have been developed as alternatives to Pt-based catalysts for HER in acidic medium. Two main types of carbon-based HER catalysts with low overpotentials and good durability have been developed, including nonmetal doped carbon and metal@carbon. In this feature article, we review the research progress in the development of carbon-based electrocatalysts toward HER throughout the past few years. Continuing breakthroughs about carbon-based electrocatalysts have revealed innovative catalysts with improved HER performance. However, several unanswered questions about carbon-based electrocatalysts toward HER need be systematically researched, such as controllable synthesis of metal@carbon, catalytic mechanism, etc. (1) As for nonmetal doped carbon, the enhanced catalytic activity for HER was interpreted by the same mechanism for ORR in most papers. Up to now, the reported results about nonmetal types and doping sites into carbon were limited, which can not provide the accurate laws to design the efficient HER catalysts. For example, N doped carbons as efficient catalysts were widely used in ORR, however, not all N-doped carbons possess the high performance for HER. Usually, there are some possible metal impurities in nonmetal doped carbon, which will enhance the HER performance of nonmetal doped carbon. In fact, the single-atom Co and Ni doped into carbon as efficient HER electrocatalysts have been developed [23,57]. (2) As for metal@carbon, the core metals have been restricted to only a small number of transition metals, such as Fe, Co and Ni. Thus, extending the core metal to other metals is the valuable research content in the future, which will give more information to analyze the catalytic activity caused by different electronic structure. In addition, the controllable thickness and component of shell structures should be established to confirm the catalytic sites from metal core or carbon shell. At last, the above mechanism was proposed by DFT calculations. So, more experimental results need to give more direct evidences. (3) Electrochemistry, especially for activation process. The activation treatment for enhancing HER performance in electrochemical measurement with Pt as counter electrode should be used with caution. However, if eliminating the dissolution of Pt, the overpotentials for HER were also markedly improved after the activation, the mechanism should be researched, can not be simply attributed to the full infiltration between electrolyte and electrode. (4) OER in acidic electrolyte. The acidic electrolytes (e.g. 0.5 M H_2SO_4) are preferred for water electrolysis to produce hydrogen as there are enough H^+ ions in the electrolyte to react on the electrode surface. Up to now, significant research efforts have been devoted to the design and engineering of acid-stable HER catalysts. However, for the final industrial application, it is also essential to develop the electrolysis of water through two electrodes, anode for OER and cathode for HER. Hence, in the next step, the development of OER catalysts with high performance in acidic electrolyte is extremely urgent. Unfortunately, few results about the efficient catalysts for OER in acidic electrolyte have been reported [95,96].

Acknowledgments

This work was supported by the National Recruitment Program of Global Experts, Project of Public Interest Research and Capacity Building of Guangdong Province (2014A010106005), Excellent Youth Foundation of Guangdong Scientific Committee (S2013050013882), the National Natural Science Foundation of China (51502096), and the National Science Fund for Excellent Young Scholars of China (51422203).

References

[1] J. Luo, J.H. Im, M.T. Mayer, M. Schreier, M.K. Nazeeruddin, N.G. Park, S.D. Tilley, H.J. Fan, M. Grätzel, Science 345 (2014) 1593–1596.
[2] E.J. Popczun, J.R. Mckone, C.G. Read, A.J. Biacchi, A.M. Wiltrout, N.S. Lewis, R. E. Schaak, J. Am. Chem. Soc. 135 (2013) 9267–9270.
[3] R. Sathre, C.D. Scown, W.R. Morrow, J.C. Stevens, I.D. Sharp, J.W. Ager, K. Walczak, F.A. Houle, J.B. Greenblatt, Energy Environ. Sci. 7 (2014) 3264–3278.
[4] J.R. Varcoe, P. Atanassov, D.R. Dekel, A.M. Herring, M.A. Hickner, P.A. Kohl, A. R. Kucernak, W.E. Mustain, K. Nijmeijer, K. Scott, T. Xu, L. Zhuang, Energy Environ. Sci. 7 (2014) 3135–3191.
[5] M. Zeng, Y. Li, J. Mater. Chem. A 3 (2015) 14942–14962.
[6] J. Deng, P. Ren, D. Deng, L. Yu, F. Yang, X. Bao, Energy Environ. Sci. 7 (2014) 1919–1923.
[7] Y. Su, Y. Zhu, H. Jiang, J. Shen, X. Yang, W. Zou, J. Chen, C. Li, Nanoscale 6 (2014) 15080–15089.
[8] M.G. Walter, E.L. Warren, J.R. Mckone, S.W. Boettcher, Q. Mi, E.A. Santori, N. S. Lewis, Chem. Rev. 110 (2010) 6446–6473.
[9] C.G.M. Guio, L.A. Stern, X. Hu, Chem. Soc. Rev. 43 (2014) 6555–6569.
[10] W. Zhou, K. Zhou, D. Hou, X. Liu, G. Li, Y. Sang, H. Liu, L.G. Li, S. Chen, ACS Appl. Mater. Interfaces 6 (2014) 21534–21540.
[11] D. Gopalakrishnan, D. Damien, M.M. Shaijumon, ACS Nano 8 (2014) 5297–5303.
[12] W. Zhou, D. Hou, Y. Sang, S. Yao, J. Zhou, G. Li, L. Li, H. Liu, S. Chen, J. Mater. Chem. A 2 (2014) 11358–11364.
[13] X. Ge, L. Chen, L. Zhang, Y. Wen, A. Hirata, M. Chen, Adv. Mater. 26 (2014) 3100–3104.
[14] C. Wan, Y.N. Regmi, B.M. Leonard, Angew. Chem. Int. Ed. 53 (2014) 6407–6410.
[15] Z. Xing, Q. Liu, A.M. Asiri, X. Sun, Adv. Mater. 26 (2014) 5702–5707.
[16] L. Cheng, W. Huang, Q. Gong, C. Liu, Z. Liu, Y. Li, H. Dai, Angew. Chem. Int. Ed. 53 (2014) 7860–7863.
[17] D. Kong, H. Wang, Z. Lu, Y. Cui, J. Am. Chem. Soc. 136 (2014) 4897–4900.
[18] M.S. Faber, R. Dziedzic, M.A. Lukowski, N.S. Kaiser, Q. Ding, S. Jin, J. Am. Chem. Soc. 136 (2014) 10053–10061.
[19] J. Tian, Q. Liu, A.M. Asiri, X. Sun, J. Am. Chem. Soc. 136 (2014) 7587–7590.
[20] M. Li, X. Liu, Y. Xiong, X. Bo, Y. Zhang, C. Han, L. Guo, J. Mater. Chem. A 3 (2015) 4255–4265.
[21] X. Fan, Z. Peng, R. Ye, H. Zhou, X. Guo, ACS Nano 9 (2015) 7407–7418.
[22] X. Zou, X. Huang, A. Goswami, R. Silva, B.R. Sathe, E. Mikmekova, T. Asefa, Angew. Chem. Int. Ed. 53 (2014) 4372–4376.
[23] H.J. Qiu, Y. Ito, W. Cong, Y. Tan, P. Liu, A. Hirata, T. Fujita, Z. Tang, M. Chen, Angew. Chem. Int. Ed. 127 (2015) 14237–14241.
[24] Y. Zheng, Y. Jiao, L.H. Li, T. Xing, Y. Chen, M. Jaroniec, S.Z. Qiao, ACS Nano 8 (2014) 5290–5296.
[25] Y. Zhou, W. Zhou, D. Hou, G. Li, J. Wan, C. Feng, Z. Tang, S. Chen, Small 12 (2016) 2768–2774.
[26] M. Zeng, Y. Li, J. Mater. Chem. A 3 (2015) 14942–14962.
[27] T. Wang, Q. Zhou, X. Wang, J. Zheng, X. Li, J. Mater. Chem. A 3 (2015) 16435–16439.
[28] W. Zhou, Y. Zhou, L. Yang, J. Huang, Y. Ke, K. Zhou, L. Li, S. Chen, J. Mater. Chem. A 3 (2015) 1915–1919.
[29] J. Duan, S. Chen, M. Jaroniec, S.Z. Qiao, ACS Nano 9 (2015) 931–940.
[30] Y. Ito, W. Cong, T. Fujita, Z. Tang, M. Chen, Angew. Chem. Int. Ed. 54 (2015) 2131–2136.
[31] K. Zeng, D. Zhang, Prog. Energy Combust. Sci. 36 (2010) 307–326.
[32] Y. Yan, B. Xia, Z. Xu, X. Wang, ACS Catal. 4 (2014) 1693–1705.
[33] F. Jiao, H. Frei, Energy Environ. Sci. 3 (2010) 1018–1027.
[34] J. Yang, H.S. Shin, J. Mater. Chem. A 2 (2014) 5979–5985.
[35] D. Merki, X. Hu, Energy Environ. Sci. 4 (2011) 3878–3888.
[36] A.B. Laursen, S. Kegnæs, S. Dahl, I. Chorkendorff, Energy Environ. Sci. 5 (2012) 5577–5591.
[37] Y. Jiao, Y. Zheng, M. Jaroniec, S.Z. Qiao, Chem. Soc. Rev. 44 (2015) 2060–2086.
[38] J. Wang, W. Cui, Q. Liu, Z. Xing, A.M. Asiri, X. Sun, Adv. Mater. 28 (2016) 215–230.
[39] Y. Zheng, Y. Jiao, S.Z. Qiao, Adv. Mater. 27 (2015) 5372–5378.
[40] B.R. Sathe, X. Zou, T. Asefa, Catal. Sci. Technol. 4 (2014) 2023–2030.
[41] L. Yang, S. Jiang, Y. Zhao, L. Zhu, S. Chen, X. Wang, Q. Wu, J. Ma, Y. Ma, Z. Hu, Angew. Chem. Int. Ed. 123 (2011) 7270–7273.
[42] J. Jin, F. Pan, L. Jiang, X. Fu, A. Liang, Z. Wei, J. Zhang, G. Sun, ACS Nano 8 (2014) 3313–3321.
[43] Z. Yang, Z. Yao, G. Li, G. Fang, H. Nie, Z. Liu, X. Zhou, X.A. Chen, S. Huang, ACS Nano 6 (2012) 205–211.
[44] J. Zhang, L. Qu, G. Shi, J. Liu, J. Chen, L. Dai, Angew. Chem. Int. Ed. 128 (2016) 2270–2274.
[45] Y. Zhao, F. Zhao, X. Wang, C. Xu, Z. Zhang, G. Shi, L. Qu, Angew. Chem. Int. Ed. 53 (2014) 13934–13939.
[46] S.S. Shinde, A. Sami, J.H. Lee, J. Mater. Chem. A 3 (2015) 12810–12819.
[47] Y. Liu, H. Yu, X. Quan, S. Chen, H. Zhao, Y. Zhang, Sci. Rep. 4 (2014) 6843.
[48] X. Huang, Y. Zhao, Z. Ao, G. Wang, Sci. Rep. 4 (2014) 7557.
[49] Y. Zheng, Y. Jiao, Y. Zhu, L.H. Li, Y. Han, Y. Chen, A. Du, M. Jaroniec, S.Z. Qiao, Nat. Commun. 5 (2014) 3783, http://dx.doi.org/10.1038/ncomms4783.
[50] L. Wei, H.E. Karahan, K. Goh, W. Jiang, D. Yu, O. Birer, R. Jiang, Y. Chen, J. Mater. Chem. A 3 (2015) 7210–7214.
[51] J. Liang, X. Du, C. Gibson, X.W. Du, S.Z. Qiao, Adv. Mater. 25 (2013) 6226–6231.
[52] L. Liao, J. Zhu, X. Bian, L. Zhu, M.D. Scanlon, H.H. Girault, B. Liu, Adv. Funct. Mater. 23 (2013) 5326–5333.
[53] M. Shalom, S. Gimenez, F. Schipper, I.H. Cardona, J. Bisquert, M. Antonietti, Angew. Chem. Int. Ed. 53 (2014) 3654–3658.
[54] D.S. Su, J. Zhang, B. Frank, A. Thomas, X. Wang, J. Paraknowitsch, R. Schlögl, ChemSusChem 3 (2010) 169–180.
[55] M. Chhetri, S. Maitra, H. Chakraborty, U.V. Waghmare, C.N.R. Rao, Energy Environ. Sci. 9 (2016) 95–101.
[56] R.K. Shervedani, A. Amini, Carbon 93 (2015) 762–773.
[57] H. Fei, J. Dong, M.J.A. Jimenez, G. Ye, N.D. Kim, E.L. Samuel, Z. Peng, Z. Zhu, F. Qin, J. Bao, M.J. Yacaman, P.M. Ajayan, D. Chen, J.M. Tour, Nat. Commun. 6 (2015) 8668, http://dx.doi.org/10.1038/ncomms9668.
[58] J. Lu, T. Xiong, W. Zhou, L. Yang, Z. Tang, S. Chen, ACS Appl. Mater. Interfaces 8 (2016) 5065–5069.
[59] J. Deng, P. Ren, D. Deng, X. Bao, Angew. Chem. Int. Ed. 54 (2015) 2100–2104.
[60] Z. Xing, Q. Liu, W. Xing, A.M. Asiri, X. Sun, ChemSusChem 8 (2015) 1850–1855.
[61] M. Tahir, N. Mahmood, X.X. Zhang, T. Mahmood, F.K. Butt, I. Aslam, M. Tanveer, F. Idrees, S. Khalid, I. Shakir, Y.M. Yan, J.J. Zou, C.B. Cao, Y.L. Hou, Nano Res. 8 (2015) 3725–3736.
[62] W. Zhou, J. Zhou, Y. Zhou, J. Lu, K. Zhou, L. Yang, Z. Tang, L. Li, S. Chen, Chem. Mater. 27 (2015) 2026–2032.
[63] D. Hou, W. Zhou, K. Zhou, Y. Zhou, J. Zhong, L. Yang, J. Lu, G. Li, S. Chen, J. Mater. Chem. A 3 (2015) 15962–15968.
[64] M. Tavakkoli, T. Kallio, O. Reynaud, A.G. Nasibulin, C. Johans, J. Sainio, H. Jiang, E.I. Kauppinen, K. Laasonen, Angew. Chem. Int. Ed. 54 (2015) 4535–4538.
[65] J. Wang, G. Wang, S. Miao, J. Li, X. Bao, Faraday Discuss 176 (2014) 135–151.
[66] S. Gao, G.D. Li, Y. Liu, H. Chen, L.L. Feng, Y. Wang, M. Yang, D. Wang, S. Wang, X. Zou, Nanoscale 7 (2015) 2306–2316.
[67] J.W. Ren, M. Antonietti, T.P. Fellinger, Adv. Energy Mater. 5 (2015) 1401660, http://dx.doi.org/10.1002/aenm.201401660.
[68] W. Zhou, T. Xiong, C. Shi, J. Zhou, K. Zhou, N. Zhu, L. Li, Z. Tang, S. Chen, Angew. Chem. Int. Ed. (2016), http://dx.doi.org/10.1002/ange.201602627.
[69] J. Lu, W. Zhou, L. Wang, J. Jia, Y. Ke, L. Yang, K. Zhou, X. Liu, Z. Tang, L. Li, S. Chen, A.C.S. Catal, 6 (2016) 1045–1053.
[70] W. Zhang, Z.Y. Wu, H.L. Jiang, S.H. Yu, J. Am. Chem. Soc. 136 (2014) 14385–14388.
[71] S. Zhao, H. Yin, L. Du, L. He, K. Zhao, L. Chang, G. Yin, H. Zhao, S. Liu, Z. Tang, ACS Nano 8 (2014) 12660–12668.
[72] X. Cao, B. Zheng, W. Shi, J. Yang, Z. Fan, Z. Luo, X. Rui, B. Chen, Q. Yan, H. Zhang, Adv. Mater. 27 (2015) 4695–4701.
[73] W. Chaikittisilp, M. Hu, H. Wang, H.S. Huang, T. Fujita, K.C.W. Wu, L.C. Chen, Y. Yamauchi, K. Ariga, Chem. Commun. 48 (2012) 7259–7261.
[74] T.Y. Ma, S. Dai, M. Jaroniec, S.Z. Qiao, J. Am. Chem. Soc. 136 (2014) 13925–13931.
[75] M. Jahan, Q. Bao, K.P. Loh, J. Am. Chem. Soc. 134 (2012) 6707–6713.
[76] J.S. Qin, D.Y. Du, W. Guan, X.J. Bo, Y.F. Li, L.P. Guo, Z.M. Su, Y.Y. Wang, Y.Q. Lan, H. C. Zhou, J. Am. Chem. Soc. 137 (2015) 7169–7177.
[77] G. Rousseau, L.M.R. Albelo, W. Salomon, P. Mialane, J. Marrot, F. Doungmene, I. M. Mbomekallé, P. De Oliveira, A. Dolbecq, Cryst. Growth Des. 15 (2015) 449–456.
[78] B. Nohra, H.E. Moll, L.M.R. Albelo, P. Mialane, J. Marrot, C.M. Draznieks, M. O'keeffe, R.N. Biboum, J. Lemaire, B. Keita, L. Nadjo, A. Dolbecq, J. Am. Chem. Soc. 133 (2011) 13363–13374.
[79] M. Jahan, Z. Liu, K.P. Loh, Adv. Funct. Mater. 23 (2013) 5363–5372.
[80] Y. Gong, Z. Hao, J. Meng, H. Shi, P. Jiang, M. Zhang, J. Lin, ChemPlusChem 79 (2014) 266–277.
[81] Y. Hou, Z. Wen, S. Cui, S. Ci, S. Mao, J. Chen, Adv. Funct. Mater. 25 (2015) 872–882.
[82] H.B. Wu, B.Y. Xia, L. Yu, X.Y. Yu, X.W. Lou, Nat. Commun. 6 (2015) 6512.
[83] T. Tian, L. Ai, J. Jiang, RSC Adv. 5 (2015) 10290–10295.
[84] Y.F. Xu, M.R. Gao, Y.R. Zheng, J. Jiang, S.H. Yu, Angew. Chem. Int. Ed. 52 (2013) 8546–8550.
[85] M.R. Gao, J.X. Liang, Y.R. Zheng, Y.F. Xu, J. Jiang, Q. Gao, J. Li, S.H. Yu, Nat. Commun. 6 (2015) 5982, http://dx.doi.org/10.1038/ncomms6982.
[86] C.C.L. Mccrory, S. Jung, J.C. Peters, T.F. Jaramillo, J. Am. Chem. Soc. 135 (2013) 16977–16987.
[87] Y. Li, H. Wang, L. Xie, Y. Liang, G. Hong, H. Dai, J. Am. Chem. Soc. 133 (2011) 7296–7299.
[88] Y. Yang, H. Fei, G. Ruan, C. Xiang, J.M. Tour, Adv. Mater. 26 (2014) 8163–8168.
[89] E.J. Popczun, C.G. Read, C.W. Roske, N.S. Lewis, R.E. Schaak, Angew. Chem. Int. Ed. 126 (2014) 5531–5534.
[90] J.F. Callejas, C.G. Read, E.J. Popczun, J.M. Mcenaney, R.E. Schaak, Chem. Mater. 27 (2015) 3769–3774.
[91] R.K. Das, Y. Wang, S.V. Vasilyeva, E. Donoghue, I. Pucher, G. Kamenov, H. P. Cheng, A.G. Rinzler, ACS Nano 8 (2014) 8447–8456.
[92] W. Cui, Q. Liu, N. Cheng, A.M. Asiri, X. Sun, Chem. Commun. 50 (2014) 9340–9342.
[93] G. Dong, M. Fang, H. Wang, S. Yip, H.Y. Cheung, F. Wang, C.Y. Wong, S.T. Chu, J. C. Ho, J. Mater. Chem. A 3 (2015) 13080–13086.
[94] C. Zhang, Y. Hong, R. Dai, X. Lin, L.S. Long, C. Wang, W. Lin, ACS Appl. Mater. Interfaces, 7, (2015) 11648–11653.
[95] R. Frydendal, E.A. Paoli, I. Chorkendorff, J. Rossmeisl, I.E.L. Stephens, Adv. Energy Mater. 5 (2015) 1500991, http://dx.doi.org/10.1002/aenm.201500991.
[96] M. Huynh, D.K. Bediako, D.G. Nocera, J. Am. Chem. Soc. 136 (2014) 6002–6010.

Dr. Weijia Zhou completed his Ph.D. at Shandong University in 2012. He was doing research at Nanyang Technological University (NTU) in 2011. Now, Dr. Zhou is an associate professor in New Energy Research Institute, School of Environment and Energy, South China University of Technology (SCUT), China. His research interests are related to the design and synthesis of functional materials and devices for new energy conversion and storage, including photo and electro-catalytic water splitting, CO_2 reduction and supercapacitor.

Jin Jia received his Bachelor's degree (2012) and Master's degree (2015) in materials science and engineering from Henan Polytechnic University (HPU). He is currently pursuing Ph.D. degree under the supervision of Ass. Prof. Weijia Zhou and Prof. Shaowei Chen in the School of Environment and Energy at the South China University of Technology (SCUT). His current research interest focuses on the design and synthesis of nanomaterials for energy conversion and storage.

Jia Lu received her B.S. degree at South China Agriculture University in 2013, and now she is a master degree candidate at South China University of Technology (SCUT) under the supervision of Dr. Weijia Zhou and Prof. Shaowei Chen. Her research interest includes metal embedded carbon hybrid catalysts for oxygen reduction reaction and electrochemistry of water splitting.

Linjing Yang received B.S. degree from Hebei University of Technology in 2014. She is pursuing her M.D. degree under the supervision of Dr. Weijia Zhou and Prof. Shaowei Chen in New Energy Research Institute, South China University of Technology (SCUT). Her research interests include electrocatalytic water splitting and oxygen reduction.

Dongman Hou obtained her B.S. degree from School of Chemistry and Chemical Engineering, South China University of Technology in 2013. She is now pursuing her Master Degree under the supervision of Professor Guoqiang Li and Dr Weijia Zhou, South China University of Technology. Her researches focus on the fabrication and application of flexible electrodes for highly efficient hydrogen evolution.

Prof. Guoqiang Li received his Ph.D. degree of materials science at Northwestern Polytechnical University, Xi'an, China, in 2004. Afterwards, he joined GE Global Research as an R&D scientist, and then carried out two postdoctoral research experiences in University of Tokyo (2005–2007) under the JSPS fellowship, and University of Oxford (2007–2010) under the Royal Society International Incoming Fellowship. He has been a full professor at South China University of Technology, China since 2010. Prof. Li has broad interests in synthesis of compound semiconductor materials and fabrication of relevant devices. He has published over 100 peer-reviewed articles and patented over 40 techniques.

Dr. Shaowei Chen obtained a B.Sc. degree from the University of Science and Technology of China, and then went to Cornell University receiving his M.Sc. and Ph.D. degrees in 1993 and 1996. Following a postdoctoral appointment in the University of North Carolina at Chapel Hill, he started his independent career in Southern Illinois University in 1998. In 2004, he moved to the University of California at Santa Cruz and is currently a Professor of Chemistry. He is also an adjunct professor at South China University of Technology. His research interest is primarily in the electron transfer chemistry of nanoparticle materials.